Geophysical Research Letters

RESEARCH LETTER
10.1029/2018GL080077

Key Points:
- A filtering step in conversion to I/F can cause few-pixel artifacts in high variance regions of a CRISM image cube
- Orbital detections of perchlorate and some serpentine on Mars may not be robust, instead caused by the newly discovered artifact
- Few-pixel mineral detections using visible-shortwave infrared reflectance spectroscopy should be confirmed with radiance data

Supporting Information:
- Supporting Information S1
- Figure S1
- Figure S2
- Figure S3
- Figure S4
- Figure S5
- Figure S6
- Figure S7
- Figure S8
- Figure S9
- Figure S10
- Figure S11
- Figure S12
- Figure S13
- Figure S14
- Figure S15
- Figure S16
- Figure S17
- Table S1

Correspondence to:
E. K. Leask,
eleask@caltech.edu

Citation:
Leask, E. K., Ehlmann, B. L., Dundar, M. M., Murchie, S. L., & Seelos, F. P. (2018). Challenges in the search for perchlorate and other hydrated minerals with 2.1-μm absorptions on Mars. *Geophysical Research Letters, 45*, 12,180–12,189. https://doi.org/10.1029/2018GL080077

Received 17 AUG 2018
Accepted 5 NOV 2018
Accepted article online 9 NOV 2018
Published online 26 NOV 2018

Challenges in the Search for Perchlorate and Other Hydrated Minerals With 2.1-μm Absorptions on Mars

E. K. Leask[1], B. L. Ehlmann[1,2], M. M. Dundar[3], S. L. Murchie[4], and F. P. Seelos[4]

[1]Division of Geological and Planetary Sciences, California Institute of Technology, Pasadena, California, USA, [2]Jet Propulsion Laboratory, California Institute of Technology, Pasadena, California, USA, [3]Computer and Information Sciences Department, Indiana University-Purdue University at Indianapolis, Indianapolis, Indiana, USA, [4]Johns Hopkins University/Applied Physics Laboratory, Laurel, Maryland, USA

Abstract A previously unidentified artifact has been found in Compact Reconnaissance Imaging Spectrometer for Mars targeted I/F data. It exists in a small fraction (<0.05%) of pixels within 90% of images investigated and occurs in regions of high spectral/spatial variance. This artifact mimics real mineral absorptions in width and depth and occurs most often at 1.9 and 2.1 μm, thus interfering in the search for some mineral phases, including alunite, kieserite, serpentine, and perchlorate. A filtering step in the data processing pipeline, between radiance and I/F versions of the data, convolves narrow artifacts ("spikes") with real atmospheric absorptions in these wavelength regions to create spurious absorption-like features. The majority of previous orbital detections of alunite, kieserite, and serpentine we investigated can be confirmed using radiance and raw data, but few to none of the perchlorate detections reported in published literature remain robust over the 1.0- to 2.65-μm wavelength range.

Plain Language Summary Many minerals can be identified with remote sensing data by their characteristic absorptions in visible-shortwave infrared data. This type of data has allowed geological interpretation of much of Mars' surface, using satellite-based observation. We have discovered an issue with the Compact Reconnaissance Imaging Spectrometer for Mars instrument's data processing pipeline. In ~ <0.05% of pixels in almost all images, noise in the data is smoothed in such a way that it mimics real mineral absorptions, falsely making it look as though certain minerals are present on Mars' surface. The vast majority of previously identified minerals are still confirmed after accounting for the artifact, but some to all perchlorate detections and a few serpentine detections were not confirmed, suggesting that the artifact created false detections. This means concentrated regions of perchlorate may not occur on Mars and so may not be available to generate possibly habitable salty liquid water at very cold temperatures.

1. Introduction

The Compact Reconnaissance Imaging Spectrometer for Mars (CRISM) aboard the Mars Reconnaissance Orbiter has been collecting visible/shortwave infrared reflectance data (0.4–3.9 μm) since 2006 (Murchie et al., 2007). These data have revolutionized our knowledge of Mars' surface, allowing the identification of mafic, hydrated, and evaporite mineral deposits as well as interpretation of the geological processes that created them (e.g., Bishop, Dobrea, et al., 2008; Carter et al., 2013; Ehlmann et al., 2008; Murchie, Mustard, et al., 2009; Mustard et al., 2008; Wray et al., 2011). There are several known artifacts in the CRISM data set that must be taken into consideration when analyzing data, including a sharp feature created by a filter boundary at 1.65 μm and a "sawtooth" pattern caused by imperfect atmospheric correction at ~2 μm (Murchie, Seelos, et al., 2009; Wiseman et al., 2016). Nonetheless, the data quality is sufficient to discover minerals previously unreported for Mars, map their distribution, and generate new insights into Martian environmental processes.

We began this work thinking we had discovered a hydrated phase with a 2.1-μm absorption in some ways similar to perchlorate, present in small exposures widely scattered across the surface of Mars. Upon further investigation, we discovered that it was a previously undescribed artifact, present in a small fraction of I/F (π × radiance from the surface divided by solar irradiance) pixels in ~90% of CRISM images investigated. It mimics the characteristics of real mineral absorptions, covering ~20 consecutive bands, and arises from incomplete handling of spikes in the radiance data by a noise filtration step in the radiance to I/F conversion (Figures 1b and 1c).

This artifact creates challenges when searching for mineral phases on Mars, especially those with absorptions in the 1.9- and 2.1-μm wavelength range, as we have found that the most frequent multiband artifacts occur

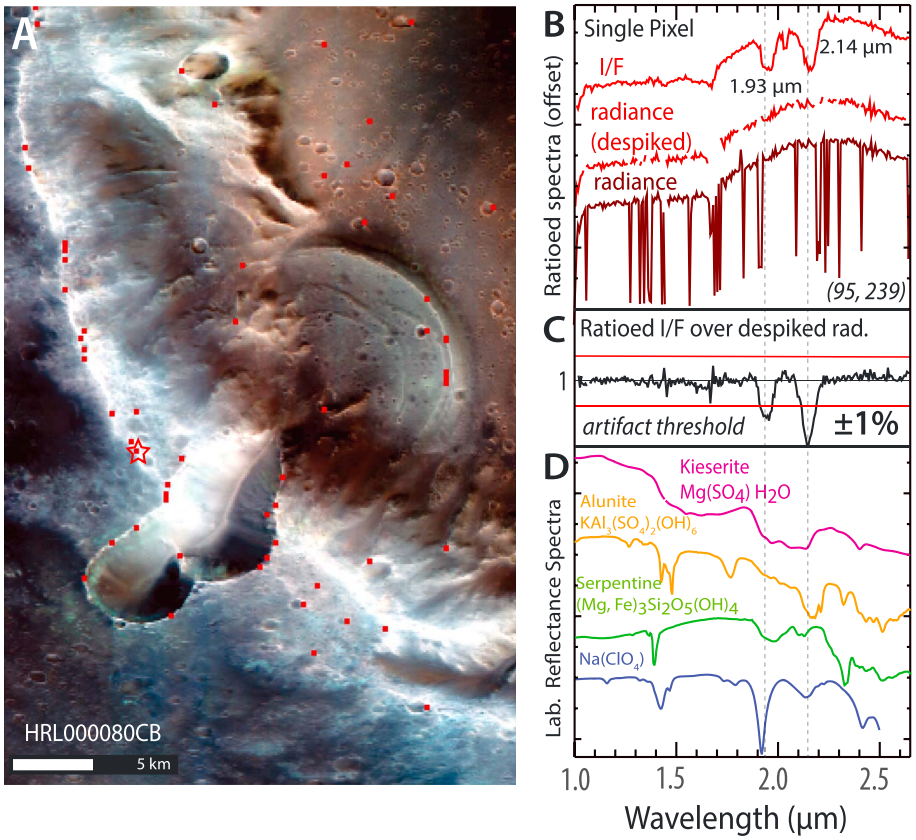

Figure 1. Example of the (a) spatial and (b) spectral appearance of the artifact creating the spurious absorptions, shown in ratioed I/F and ratioed radiance. (c) The threshold for an artifact is defined to be where ratioed radiance differs from ratioed I/F by more than 1%. (d) Laboratory spectra of minerals with a 2.1-μm absorption are shown for comparison (from USGS spectral library (Clark et al. (2007)) and Hanley et al. (2015)).

at these wavelengths. Minerals whose detections might be affected include the hydrated and/or hydroxylated phases kieserite, alunite, serpentine, and perchlorate, each of which has specific implications for the geochemical conditions present at the time of formation. Here we describe the steps taken to identify the artifact and characterize its distribution in the CRISM data set. We revisit key previously reported detections of key mineral phases potentially impacted by this artifact by examining whether apparent absorptions persist in less processed data products (radiance and raw data), which were not subjected to noise filtering. Finally, we recommend data processing approaches that mitigate the effects of the artifact on CRISM data interpretation.

2. Materials and Methods

This artifact, which we will refer to as a "spurious absorption," was first discovered with a multistep Bayesian clustering algorithm designed to automate detection of rare minerals in CRISM images (implemented by Yerebakan et al. (2014) and Dundar and Ehlmann (2016)). To understand the origin of observed spectral features, we analyzed raw and radiance data in addition to I/F. We employ these earlier data products in the processing pipeline to verify absorption features and differentiate between real features and pipeline-generated artifacts (for details, see supporting information). Although radiance and raw data are noisy, robust mineral detections can be seen in all types of ratioed data (e.g., Figure S15).

The CRISM data processing pipeline includes a filtering step between radiance and I/F (Murchie et al., 2016, Appendix N). This filtering is designed to remove sharp, narrow "spikes" in the radiance data set. Spikes can be positive or negative, and often result from a lag in the response of a detector element when crossing an abrupt brightness boundary (Figures 1b and S4). Throughout this paper, we use "spike" to mean an abrupt departure from the continuum value, with a maximum of three consecutive channels (most often 1).

Spikes are generated where particular detector elements are slower than their neighbors in recording an abrupt spatial change in surface brightness. Unlike spikes, "spurious absorptions" (or "absorption-like features") are typically present over ~20 channels, and have gradual shoulders on either side of the main departure from the continuum value. We present spectra as ratioed data for ease of comparison between data sets; for ratioing, we use a "bland" denominator spectrum constructed from pixels within the same detector column in an image (unless otherwise indicated, bland denominators are simple column medians).

3. Results and Discussion

Pixels with 1.9- and 2.1-μm absorptions were identified in 317 of 344 CRISM images examined from across the surface of Mars (Figure S1 and Table S1); another 6 images contained potential identifications, and 21 contained none. To verify whether the apparent absorptions at 1.9 and 2.1 μm were real surface features, we first confirmed that they were present in unratioed I/F data (and not introduced by the choice of denominator). The same spectral features were also confirmed present in advanced products derived from I/F, including targeted empirical records and map-projected targeted reduced data records. The apparent absorptions were present after every iteration of atmospheric correction available in CAT-ENVI, and could be seen even in raw I/F data prior to atmospheric correction.

Next, we checked whether our observed 1.9- and 2.1-μm paired absorption-like features occurred in places that were geologically plausible. Our pixels tend to occur scattered in single- or few-pixel groups in areas of topographic roughness, following edges of geologic features (see Figures 1a and S4). This spatial pattern is unusual, as mineral deposits tend to be found in larger clusters; however, real mineral deposits could plausibly follow topographic features, if erosion were exposing a unique composition from beneath dust. We also observed pixels with paired 1.9- and 2.1-μm spectral features present at rover sites, although corresponding areas of unique composition near traverses have not been flagged by Curiosity or Opportunity. We found a similar spectral pattern in active basaltic dunes at Nili Patera, and seasonal CO_2 frost in Russell crater. Concentrated hydrated or hydroxylated mineral deposits large enough to be observable from orbit are unlikely to occur within active dunes or seasonal frost, so we began to suspect that the 1.9- and 2.1-μm spectral features might not originate from a real surface phase. We also checked images taken from the 2007 global dust storm—because this is thoroughly mixed dust, we should not see any concentrated mineral phase. The 1.9- and 2.1-μm paired spectral pattern was not found in the dust storm. However, the dust storm images also lacked any areas of strong brightness contrast, as the surface was wholly obscured by dust.

Images with no or potential spurious absorptions usually contained very few areas of strong brightness contrast. The image subset included images from the early part of the mission (2006–2008) as well as images from later in the mission (up to 2014), where IR data became noisier due to reduced cryocooler function (Figure S2). No clear trend was observed between the number of artifacts detected per image through time. A typical image contains 50–100 "artifact" pixels, as selected by our automated algorithm (see S1.1 and Figure 2a). Spatially contiguous individual artifact detections were almost all in the 1–3 pixel range with a maximum size of 12 contiguous pixels (Figure S3).

3.1. Characteristics of the Apparent "2.1-μm Absorption"

Real mineral phases have consistent spectral characteristics, including shape, depth, and central wavelength of absorptions; changes in the mineral formula (e.g., solid solution) or mixtures of multiple phases cause systematic variations. In pixels with spectra consistent with our potential mineral phase, we see absorption-like features consistently at 1.9 and 2.1 μm, occasionally with other features at 1.5 and 2.5 μm. The relative depths of the absorption-like features vary, and the band center at ~2.1 μm ranges from 2.10 to 2.16 μm, without any other systematic changes in spectral properties that might be expected of a changing composition. When we searched outside the automated pixel detections, we found that strong absorption-like features were sometimes present alone at 1.9 or 2.1 μm, less often at ~2.5 μm, and occasionally elsewhere in the spectrum (Figures S5e and S5f). We did not systematically evaluate the 2.8–3.9-μm-wavelength region due to elevated transient noise effects in this low-signal spectral region (see S2).

3.2. Comparison of Ratioed I/F and Ratioed Radiance Data

To evaluate the validity of these absorption-like features, we compared ratioed I/F spectra to ratioed radiance data on a pixel-by-pixel basis to ascertain whether the absorption at 2.1 μm persisted in radiance data. While

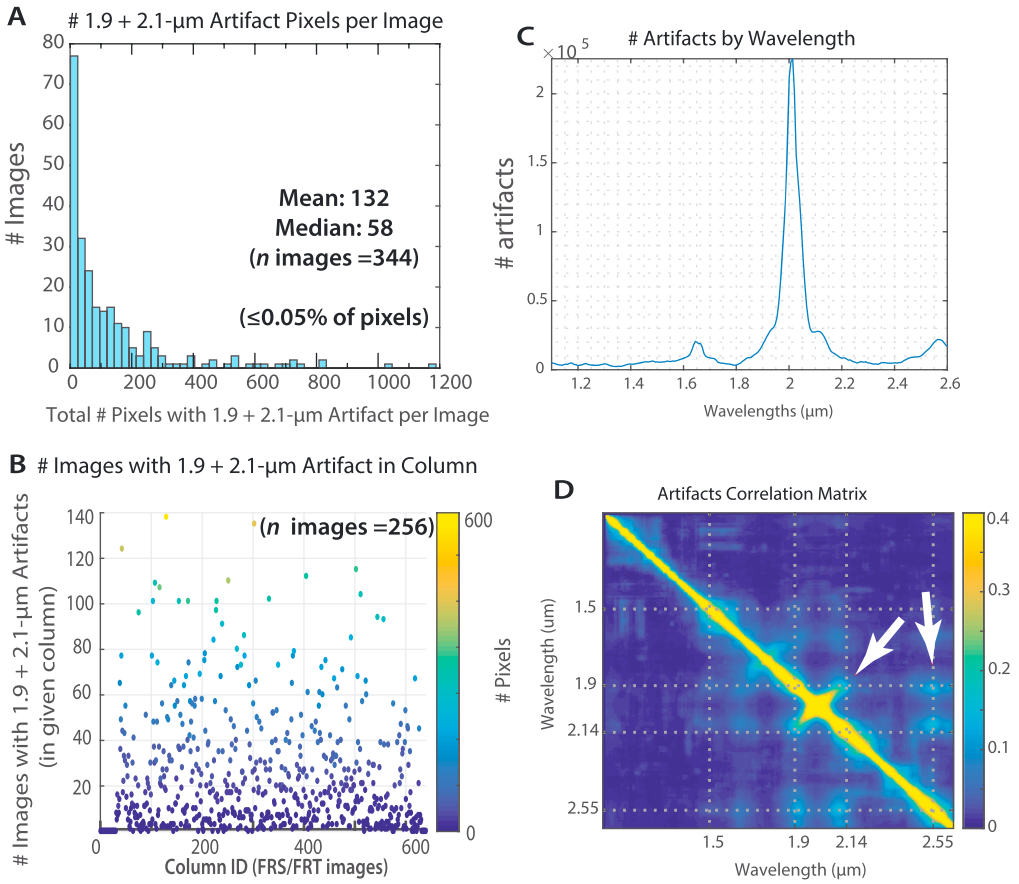

Figure 2. Characterization of artifact properties. (a) The distribution of the number of artifacts at 1.9 and 2.1 μm (selected by our algorithm) per image is shown in; most images have tens to hundreds of artifacts. (b) These artifacts at 1.9 and 2.1 μm occur preferentially in certain columns across many images. Panels on the right aggregate data for 21 images processed from radiance data. (c) The total number of artifacts at each wavelength in all the images processed. (d) A correlation matrix for the same data set. Off-axis hot spots in this matrix show where artifacts at different wavelengths tend to co-occur in the same pixels, notably at 1.9, 2.1, and 2.5 μm (arrows).

spectra of valid mineral detections appear similar in ratioed I/F and ratioed radiance (Figures 3a and S15), the strong absorptions at 2.1 μm in ratioed I/F in pixels selected by our algorithm do not persist in ratioed radiance (Figures 1b and S5c). For a representative subset of images, every pixel identified with our algorithm as having this 2.1-μm spectral signature was examined to see if the feature was present in ratioed radiance data. In every case, instead of the feature at 2.1 μm, we found spikes in ratioed radiance data.

3.3. Trends in Spikes and Artifacts

As our initial Bayesian detection algorithm was tuned to find absorptions at 2.1 μm, we searched for similar spurious absorptions at other wavelengths by comparing ratioed I/F and ratioed radiance for 21 images to generate statistics for spectral positions of spikes, spike clusters, and artifacts (Figures 2c, 2d, S5, and S6). We also looked for wavelength dependence in spikes or clusters of spikes in the radiance data because the spatial distribution of spikes, spike clusters, and artifacts appeared to be similar (Figure S4).

3.3.1. Wavelength Dependence of Spikes in Radiance Data

To identify single- to few-channel spikes in ratioed radiance data we employed a two-step median filter. For each single-pixel spectrum, the data were compared to a wide (30-band) median filter, and values that differed more than 5% from the median were excluded (obvious spikes). A second (four-band) median filter was then applied, and values that differed more that 1% from this second median were excluded. Although this procedure is effective for identifying spikes, despiked data must be used with care as real narrow absorptions are occasionally misclassified as spikes. For each cube examined, spikes were most common at 1.65 μm (a known filter boundary artifact) and ~2 μm (the "center" of the atmospheric CO_2 triplet) (Figures S5a and

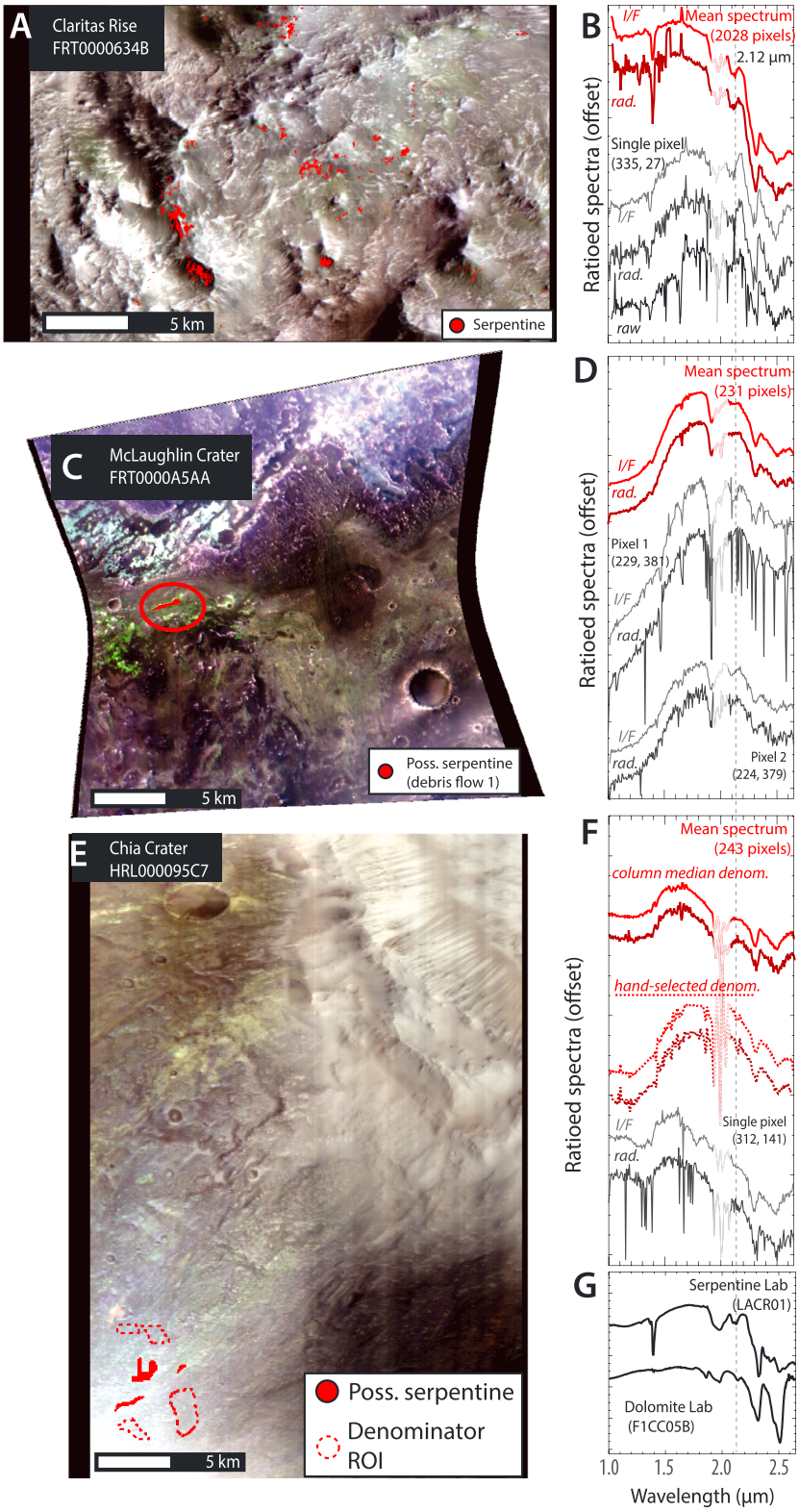

Figure 3. Analysis of previously reported serpentine detections. (a and b) Serpentine detections at Claritas rise remain robust in radiance data in single-pixel and mean spectra. Mean spectra for proposed serpentine detections at (c and d) McLaughlin and (e and f) Chia craters show marginal 2.12-μm absorptions when examined in radiance data. At McLaughlin, some of the proposed serpentine pixels retain a 2.12-μm absorption in radiance data ((d), pixel 2) while others are clearly artifacts ((d), pixel 1). At Chia crater, none of the single pixels examined have a robust 2.12-μm absorption in radiance data when basic column-median ratios are used. However, when spectrally bland regions selected by hand are used for the denominator, a narrow 2.12-μm absorption persists in radiance data.

S5b; compare to CO_2 (g) spectrum, Figure S13c). At longer wavelengths (~2.4–2.65 μm), spikes and clusters of spikes become more common. (Here a "cluster" is defined as at least 4 spikes within an 11-band spectral interval (Figure S5).) However, neither spikes nor clusters of spikes preferentially occur at either 1.9 or 2.1 μm. No correlations between spikes at 1.9 and 2.1 μm or any other wavelengths are observed (Figures S6a–S6c).

3.3.2. Wavelength Dependence of Spurious Absorptions

We searched for all spurious absorption-like features by dividing the ratioed I/F by despiked ratioed radiance; ideally, this ratio should be equal to 1. Bands were identified as containing an artifact if the ratio diverged from unity by >1% (Figure 1c). Artifacts occur most commonly at 1.65, 2.0 (extending to 1.9 and 2.1 μm), and 2.5 μm (Figures 2c, S5e, and S5f). Unlike spikes and spike clusters, artifacts centered at different wavelengths do show off-axis trends in the correlation matrix, co-occurring at 1.9, 2.14, and 2.55 μm (Figures 2d, S6e, and S6f).

3.4. "Bad" Detector Elements

While pixels selected by our algorithm are found scattered throughout images, there are some columns (corresponding to detector elements) in which artifacts at 1.9 and 2.1 μm occur repeatedly in many images (Figure 2b). This suggests that certain detector elements are more prone to detector lag (radiance spikes) in these parts of the spectrum. Of 256 full-resolution images investigated, several columns contain artifacts at these wavelengths in more than 100 different images.

4. Assessment of Previous Mineral Detections Using the 2.1-μm Region

The 1.9-μm absorption indicates surface-adsorbed or mineral-bound water (Hunt, 1977) and occurs in many regions of Mars (e.g., Gendrin et al., 2005; Poulet et al., 2005). The 2.1-μm absorption is far rarer, and related to the presence of either H_2O or OH. Its presence—coupled with other absorption features—has specific implications for the presence of particular mineral species and their genetic environments. We assessed previously reported mineral detections that utilize the 2.1-μm region to verify whether this artifact may have affected previously reported work, examining radiance data for CRISM scenes with monohydrated sulfate, alunite, serpentine, and possible perchlorate.

4.1. Kieserite

Kieserite is a monohydrated magnesium sulfate ($MgSO_4{\cdot}H_2O$), and on Earth it is formed (a) in evaporative basins, (b) through burial and heating of polyhydrated sulfate (at least a few kilometers depth; Roach et al., 2009), or (c) by conversion of polyhydrated sulfate by low water activity groundwater. The detection of kieserite and its discrimination from other phases relies on detection of absorptions at ~1.6, 2.1, and 2.4 μm (Cloutis et al., 2006; Gendrin et al., 2005; Hunt, 1971). We examined the CRISM-type spectral region, which is typical of other reported deposits (Roach et al., 2010; Viviano-Beck et al., 2015). Kieserite is found in a large, contiguous deposit (Figure S7). Because all absorptions necessary for identification are present in the mean spectrum of all stages of CRISM data, the identification of kieserite in this image is not affected by the 2.1-μm artifact. This is the case for the majority of previously reported kieserite detections on Mars which span hundreds of pixels, whereas the artifact affects only up to ~12 contiguous pixels.

4.2. Alunite

Alunite is a hydroxylated aluminum sulfate mineral ($KAl_3(SO_4)_2(OH)_6$) which forms in acidic conditions, either connected to magmatic fluids or as a product of acidic alteration (Ehlmann et al., 2016, and references therein). The detection of alunite and its discrimination from other phases relies on detection of an absorption at 2.17 μm, a doublet at 1.43 and 1.48 μm, and weaker absorptions at 1.76, 2.32, and 2.52 μm (e.g., Swayze et al., 2006). We examined all three alunite detections currently reported in the peer-reviewed literature: the CRISM-type spectral region (Viviano-Beck et al., 2014; Ehlmann et al., 2016), a second region from Ehlmann et al. (2016)/Carter et al. (2013), and the mixed alunite deposit in Wray et al. (2011). For all three exposures, we found that alunite's diagnostic absorptions persisted in both ratioed I/F and ratioed radiance data (Figures S8–S10).

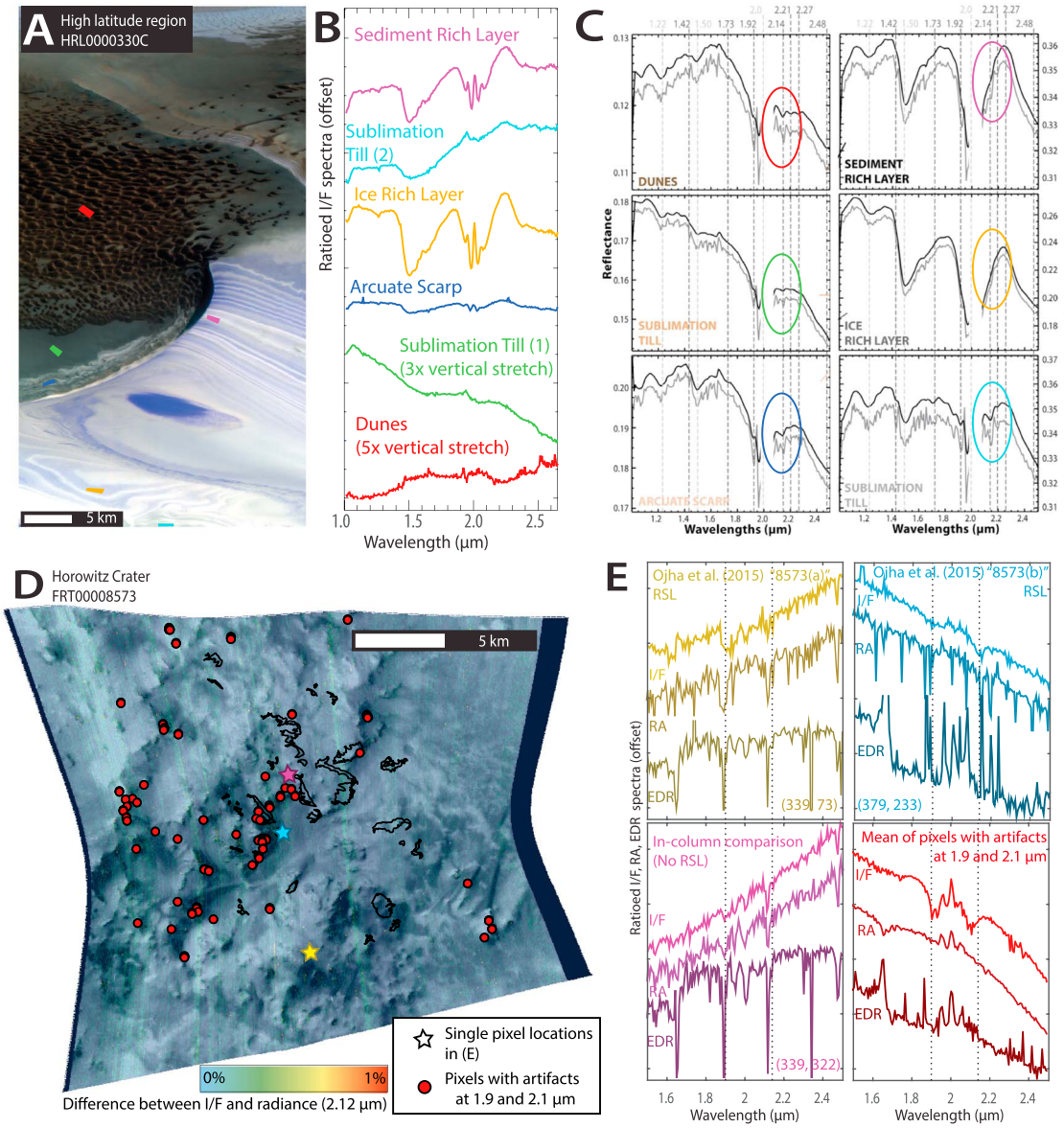

Figure 4. (a–c) Potential perchlorate detections at high-latitudes and (d and e) associated with recurring slope lineae (RSL). (a) We approximate the regions of interest presented in Massé et al. (2010). (b) Mean spectra are ratioed to column averages that exclude ice-rich regions. (c) Unratioed spectra of the regions presented in Massé et al. (2010) as possible perchlorates show a small absorption at 2.14 μm, which disappears in ratioed spectra in (b); it may be a result of an imperfect atmospheric correction. (d) Horowitz crater, showing distribution of RSLs, pixels with artifacts, and proposed single-pixel perchlorate detections in from Ojha et al. (2015). Corresponding spectra in (e) show that potential absorptions in single-pixel spectra are coincident with column-dependent spikes in raw data. Other artifact pixels are found throughout the image (not correlated with RSL), and the apparent absorptions in I/F do not persist in radiance or raw data (red; (e)).

4.3. Serpentine

Serpentine forms when ultramafic rocks are hydrothermally altered in waters with low silica activity (<400 °C; Evans, 2004). Serpentine has absorptions at 1.38, 2.32, and 2.52 μm, and its discrimination from other Mg phyllosilicates and mixtures of phyllosilicates and carbonates requires identification of a weaker 2.10–2.12-μm absorption (e.g., Bishop, Lane, et al., 2008; Ehlmann et al., 2010). We were able to reproduce spatially contiguous areas (>24 pixels) with a clear serpentine signature in ratioed radiance data from some previously published locations near the Claritas Rise and Nili Fossae (Figures 3a, 3b, S11, and S12). However, previously reported serpentine spectral signatures from McLaughlin crater (Figures 3c and 3d; Michalski et al., 2013) and Chia crater (Figures 3e and 3f; Ehlmann et al., 2010) become considerably less diagnostic of the presence of serpentine. The relative depth of the 2.3- and 2.5-μm features

could also be consistent with carbonate (e.g., Gaffey, 1986) rather than serpentine or a mixture spectrally dominated by nonserpentine.

4.4. Perchlorates

Hydrated chlorine salts (e.g., perchlorates) are found in hyperarid conditions in trace amounts on Earth (≤0.6 wt %; Ericksen, 1981). On Mars, they were measured at 0.4–0.6 wt % by the Phoenix lander (Hecht et al., 2009) and are also indicated at 0.05–1.05 wt % in multiple samples measured by MSL (Sutter et al., 2017). Perchlorate minerals can depress the melting point of water to 204 K (Hanley et al., 2012), and so have been put forth as a way to maintain liquid brines on the Martian surface. They can have multiple cations and are identified by absorptions at 1.43, 1.92, 2.14, and 2.42 μm (sodium perchlorate; Hanley et al., 2015). We examined results from two prior studies that reported detection of hydrated oxychlorine salts, possibly perchlorates and/or chlorates, in remote sensing data (Massé et al., 2010; Ojha et al., 2015).

4.4.1. High-Latitude Perchlorates?

Massé et al. (2010) examined unratioed I/F data from Observatoire pour la Minéralogie, l'Eau, les Glaces, et l'Activité and CRISM, and found that about 30% of the pixels in a CRISM northern polar image (FRT0000330C) have a small absorption at 2.14 μm, which they suggested might be due to perchlorate (Figure 4c). They used the targeted reduced data record, version 2 data available at the time. We reprocessed the CRISM image using targeted reduced data record version 3 data and tested the effects of different atmospheric corrections on unratioed data. The shape and position of the 2.14-μm feature changes, and even disappears completely in some instances, depending on the correction spectrum used (Figure S13). Since there is a small absorption caused by CO_2 located at 2.15 μm (Figure S13c), we believe that this proposed perchlorate detection may be the result of an imperfect atmospheric correction. Ratioed data—both I/F and radiance—show clear ice absorptions, but no 2.14-μm absorption (Figure 4b), regardless of the choice of denominator.

4.4.2. Perchlorates in Recurring Slope Lineae?

Ojha et al. (2015) presented several possible pixel-scale detections of perchlorates from two different sites with recurring slope lineae (RSL McEwan et al., 2014), in Horowitz and Palikir craters. They found pixels with an absorption-like feature centered near ~2.14 μm (as well as 1.9 μm), and attributed the absorption to perchlorates, postulating that their source was liquid brine from the RSLs. However, our analysis shows that of these pixels (Figures 4d, 4e, S14, S16, and S17), only one might possess a narrow, shallow 2.14-μm absorption in the ratioed radiance and raw data (Figure 4e, yellow spectra). However, many other pixels in the same column as the single pixel that are far from the RSL have a similar shape, suggesting that it may be a column-dependent artifact (e.g., Figure 4e, purple spectra). Additionally, we located >100 other pixels in the same image with strong spurious 1.9- and 2.1-μm absorptions within I/F data (red; Figures 4d and 4e). When these pixels with strong apparent absorptions were investigated in radiance and raw data, the absorptions all disappeared using our data processing methods. This suggests that most minor 2.14-μm absorptions reported for RSL are likely spurious. Robust identification of hydrated chlorine salts thus should include corroboration from radiance data and the presence of a relatively broad, strong 3-μm absorption.

5. Conclusions

We have found a new artifact in CRISM I/F data that mimics the characteristics of real mineral absorptions. The "spurious absorption"-type artifact is most prevalent at 1.9 and 2.1 μm, also common at ~2.5 μm, and occurs less frequently throughout the 1.0–2.65-μm wavelength range examined. It occurs as scattered single- or few-pixel clusters in ~90% of the >300 images we investigated. It appears to be related to the interaction between areas of high spectral or spatial variance in radiance, and a data-filtering step designed to remove spikes that is thresholded by the local variance. The spurious absorptions are most prevalent at 1.9 and 2.1 μm because of the interaction of real atmospheric absorptions and the filtering procedure designed to remove the spikes, creating spurious absorptions in adjacent channels which mimic spectral characteristics of real features.

Previously reported detections that utilize the 2.1-μm spectral region, including monohydrated sulfate, alunite, and most serpentine detections, are robust and persist in radiance spectra for most previously reported occurrences; however, a few serpentine spectra were not confirmed, and we were unable to confirm any of the published orbital perchlorate detections using the 1.0–2.65-μm wavelength range. Perchlorate has been

proposed as a way to achieve transiently wet, possibly habitable conditions at Mars' surface (Rummel et al., 2014), as well as serve as a marker for recent liquid brines (Ojha et al., 2015). As orbital detections of perchlorate require high concentrations (> ~5%), relatively large reservoirs of this mineral (compared to the Phoenix lander detections) have been invoked as a mechanism for allowing liquid water (brines) to exist at temperatures as low as −70 °C (Hanley et al., 2012), providing potentially habitable environments on modern Mars (e.g., Rampe et al., 2018). While our nondetection of perchlorate does not preclude the possibility that perchlorates exist in small amounts in Martian materials, it means that there is no orbitally identified major freezing point depressant or evaporite product. Models for RSL formation need not account for the presence of perchlorate-enriched brines, allowing for dry RSL formation mechanisms (e.g., Dundas et al., 2017; Edwards & Piqueux, 2016; Vincendon et al., 2018) or waters of different composition.

The occasional creation of spurious absorptions near atmospheric features interferes in the search for rare mineral phases, especially those such as perchlorate with absorptions in the 1.9- and 2.1-μm regions. However, in no case was the artifact observed to be contiguous over more than 12 pixels. This suggests straightforward steps to mitigate this effect for accurate identification of few-pixel-scale mineral outcrops in CRISM-targeted reduced data record version 3 I/F data: corroborate the detections using ratioed radiance data, reproduce the detections in multiple I/F images, and (for hydrated minerals) demonstrate occurrence of a 3-μm band due to molecular H_2O. Future CRISM data processing pipelines may include further optimizations to the spike-removal procedure to reduce such spurious absorptions.

Acknowledgments
Thanks to K. Seelos and M. Parente for the suggestions of tests during presentations of early versions of this work to the CRISM team. Thanks to J. Bandfield, an anonymous reviewer, and editor A. Dombard for comments that improved the manuscript. Funding for this work was provided in part by an NSERC PGS-D scholarship (E.K.L.), a NASA Habitable Worlds grant 80NSSC17K0444 and CRISM Extended Mission funding (B.L.E., E.K.L.), and support to B.L.E.'s group from the Rose Hills Foundation. A part of this research was sponsored by the National Science Foundation (NSF) under grant IIS-1252648 (CAREER) to M.M.D. The content is solely the responsibility of the authors and does not necessarily represent the official views of NSF. All CRISM data used in this paper are publicly available through the PDS node (http://ode.rsl.wustl.edu/mars/).

References

Bishop, J. L., Dobrea, E. Z. N., McKeown, N. K., Parente, M., Ehlmann, B. L., Michalski, J. R., Milliken, R. E., et al. (2008). Phyllosilicate diversity and past aqueous activity revealed at Mawrth Vallis, Mars. *Science*, *321*(5890), 830–833. https://doi.org/10.1126/science.1159699

Bishop, J. L., Lane, M., Dyar, M., & Brown, A. (2008). Reflectance and emission spectroscopy study of four groups of phyllosilicates: Smectites, kaolinite-serpentines, chlorites and micas. *Clay Minerals*, *43*(01), 35–54. https://doi.org/10.1180/claymin.2008.043.1.03

Carter, J., Poulet, F., Bibring, J. P., Mangold, N., & Murchie, S. (2013). Hydrous minerals on Mars as seen by the CRISM and OMEGA imaging spectrometers: Updated global view. *Journal of Geophysical Research: Planets*, *118*, 831–858. https://doi.org/10.1029/2012JE004145

Clark, R. N., Swayze, G. A., Wise, R., Livo, K. E., Hoefen, T., Kokaly, R. F., & Sutley, S. J. (2007). USGS digital spectral library splib06a. US geological survey, digital data series, 231, 2007.

Cloutis, E. A., Hawthorne, F. C., Mertzman, S. A., Krenn, K., Craig, M. A., Marcino, D., Methot, M., et al. (2006). Detection and discrimination of sulfate minerals using reflectance spectroscopy. *Icarus*, *184*(1), 121–157. https://doi.org/10.1016/j.icarus.2006.04.003

Dundar, M., & Ehlmann, B. L. (2016). Rare jarosite detection in CRISM imagery by non-parametric Bayesian clustering. Paper presented at the Hyperspectral Image and Signal Processing: Evolution in Remote Sensing (WHISPERS), 2016 8th Workshop on.

Dundas, C. M., McEwen, A. S., Chojnacki, M., Milazzo, M. P., Byrne, S., McElwaine, J. N., & Urso, A. (2017). Granular flows at recurring slope lineae on Mars indicate a limited role for liquid water. *Nature Geoscience*, *10*(12), 903–907. https://doi.org/10.1038/s41561-017-0012-5

Edwards, C. S., & Piqueux, S. (2016). The water content of recurring slope lineae on Mars. *Geophysical Research Letters*, *43*, 8912–8919. https://doi.org/10.1002/2016GL070179

Ehlmann, B., Mustard, J., & Murchie, S. (2010). Geologic setting of serpentine deposits on Mars. *Geophysical Research Letters*, *37*, L06201. https://doi.org/10.1029/2010GL042596

Ehlmann, B. L., Mustard, J. F., Murchie, S. L., Poulet, F., Bishop, J. L., Brown, A. J., Calvin, W. M., et al. (2008). Orbital identification of carbonate-bearing rocks on Mars. *Science*, *322*(5909), 1828–1832. https://doi.org/10.1126/science.1164759

Ehlmann, B. L., Swayze, G. A., Milliken, R. E., Mustard, J. F., Clark, R. N., Murchie, S. L., et al. (2016). Discovery of alunite in Cross crater, Terra Sirenum, Mars: Evidence for acidic, sulfurous waters. *American Mineralogist*, *101*(7), 1527–1542.

Ericksen, G. E. (1981). Geology and origin of the Chilean nitrate deposits: USGPO: For sale by the Supt. Of docs., GPO.

Evans, B. W. (2004). The serpentinite multisystem revisited: Chrysotile is metastable. *International Geology Review*, *46*(6), 479–506. https://doi.org/10.2747/0020-6814.46.6.479

Gaffey, S. J. (1986). Spectral reflectance of carbonate minerals in the visible and near infrared (O. 35–2.55 microns); calcite, aragonite, and dolomite. *American Mineralogist*, *71*(1–2), 151–162.

Gendrin, A., Mangold, N., Bibring, J.-P., Langevin, Y., Gondet, B., Poulet, F., Bonello, G., et al. (2005). Sulfates in Martian layered terrains: The OMEGA/Mars express view. *Science*, *307*(5715), 1587–1591. https://doi.org/10.1126/science.1109087

Hanley, J., Chevrier, V. F., Barrows, R. S., Swaffer, C., & Altheide, T. S. (2015). Near-and mid-infrared reflectance spectra of hydrated oxychlorine salts with implications for Mars. *Journal of Geophysical Research: Planets*, *120*, 1415–1426. https://doi.org/10.1002/2013JE004575

Hanley, J., Chevrier, V. F., Berget, D. J., & Adams, R. D. (2012). Chlorate salts and solutions on Mars. *Geophysical Research Letters*, *39*, L08201. https://doi.org/10.1029/2012GL051239

Hecht, M., Kounaves, S., Quinn, R., West, S., Young, S., Ming, D., Catling, D. C., et al. (2009). Detection of perchlorate and the soluble chemistry of Martian soil at the Phoenix lander site. *Science*, *325*(5936), 64–67. https://doi.org/10.1126/science.1172466

Hunt, G. R. (1971). Visible and near-infrared spectra of minerals and rocks. VI. Sulfides and sulfates. *Modern Geology*, *3*, 1–14.

Hunt, G. R. (1977). Spectral signatures of particulate minerals in the visible and near infrared. *Geophysics*, *42*(3), 501–513. https://doi.org/10.1190/1.1440721

Massé, M., Bourgeois, O., Le Mouélic, S., Verpoorter, C., Le Deit, L., & Bibring, J.-P. (2010). Martian polar and circum-polar sulfate-bearing deposits: Sublimation tills derived from the north polar cap. *Icarus*, *209*(2), 434–451. https://doi.org/10.1016/j.icarus.2010.04.017

McEwan, A. S., Dundas, C. M., Mattson, S. S., Toigo, A. D., Ojha, L., Wray, J. J., Chojnacki, M., et al. (2014). Recurring slope lineae in equatorial regions of Mars. *Nature Geoscience*, *7*(1), 53–58. https://doi.org/10.1038/ngeo2014

Michalski, J. R., Cuadros, J., Niles, P. B., Parnell, J., Rogers, A. D., & Wright, S. P. (2013). Groundwater activity on Mars and implications for a deep biosphere. *Nature Geoscience*, *6*(2), 133–138. https://doi.org/10.1038/ngeo1706

Murchie, S., Arvidson, R., Bedini, P., Beisser, K., Bibring, J. P., Bishop, J., Boldt, J., et al. (2007). Compact Reconnaissance Imaging Spectrometer for Mars (CRISM) on Mars Reconnaissance Orbiter (MRO). *Journal of Geophysical Research*, *112*, E05S03. https://doi.org/10.1029/2006JE002682

Murchie, S., Edward, G., & Slavney, S. (2016). Mars Reconnaissance Orbiter CRISM Data Product Software Interface Specification, version 1.3.7.4.

Murchie, S. L., Mustard, J. F., Ehlmann, B. L., Milliken, R. E., Bishop, J. L., McKeown, N. K., Noe Dobrea, E. Z., et al. (2009). A synthesis of Martian aqueous mineralogy after 1 Mars year of observations from the Mars Reconnaissance Orbiter. *Journal of Geophysical Research*, *114*, E00D06. https://doi.org/10.1029/2009JE003342

Murchie, S. L., Seelos, F. P., Hash, C. D., Humm, D. C., Malaret, E., McGovern, J. A., Choo, T. H., et al. (2009). Compact Reconnaissance Imaging Spectrometer for Mars investigation and data set from the Mars Reconnaissance Orbiter's primary science phase. *Journal of Geophysical Research*, *114*, E00D07. https://doi.org/10.1029/2009JE003344

Mustard, J. F., Murchie, S., Pelkey, S., Ehlmann, B., Milliken, R., Grant, J., Bibring, J.-P., et al. (2008). Hydrated silicate minerals on Mars observed by the Mars Reconnaissance Orbiter CRISM instrument. *Nature*, *454*(7202), 305–309. https://doi.org/10.1038/nature07097

Ojha, L., Wilhelm, M. B., Murchie, S. L., McEwen, A. S., Wray, J. J., Hanley, J., Massé, M., et al. (2015). Spectral evidence for hydrated salts in recurring slope lineae on Mars. *Nature Geoscience*, *8*(11), 829–832. https://doi.org/10.1038/ngeo2546

Poulet, F., Bibring, J.-P., Mustard, J., Gendrin, A., Mangold, N., Langevin, Y., Arvidson, R. E., et al. (2005). Phyllosilicates on Mars and implications for early Martian climate. *Nature*, *438*(7068), 623–627. https://doi.org/10.1038/nature04274

Rampe, E. B., Cartwright, J. A., McCubbin, F. M., & Osterloo, M. M. (2018). The role of halogens during fluid and magmatic processes on Mars. In *The Role of Halogens in Terrestrial and Extraterrestrial Geochemical Processes* (pp. 959–995). Cham, Switzerland: Springer.

Roach, L., Mustard, J., Murchie, S., Bibring, J. P., Forget, F., Lewis, K., Aharonson, O., et al. (2009). Testing evidence of recent hydration state change in sulfates on Mars. *Journal of Geophysical Research*, *114*, E00D02. https://doi.org/10.1029/2008JE003245

Roach, L. H., Mustard, J. F., Swayze, G., Milliken, R. E., Bishop, J. L., Murchie, S. L., & Lichtenberg, K. (2010). Hydrated mineral stratigraphy of Ius Chasma, Valles Marineris. *Icarus*, *206*(1), 253–268. https://doi.org/10.1016/j.icarus.2009.09.003

Rummel, J. D., Beaty, D. W., Jones, M. A., Bakermans, C., Barlow, N. G., Boston, P. J., et al. (2014). A new analysis of Mars "special regions": Findings of the second MEPAG Special Regions Science Analysis Group (SR-SAG2): Mary Ann Liebert, Inc. 140 Huguenot Street, 3rd Floor New Rochelle, NY 10801 USA.

Sutter, B., Mcadam, A. C., Mahaffy, P. R., Ming, D. W., Edgett, K. S., Rampe, E. B., Eigenbrode, J. L., et al. (2017). Evolved gas analyses of sedimentary rocks and eolian sediment in gale crater, mars: Results of the curiosity Rover's Sample Analysis at Mars (SAM) instrument from Yellowknife Bay to the Namib Dune. *Journal of Geophysical Research: Planets*, *122*, 2574–2609. https://doi.org/10.1002/2016JE005225

Swayze, G., Desborough, G., Clark, R., Rye, R., Stoffregen, R., Smith, K., & Lowers, H. (2006). Detection of jarosite and alunite with hyperspectral imaging: Prospects for determining their origin on Mars using orbital sensors. Paper presented at the Workshop on Martian Sulfates as Recorders of Atmospheric-Fluid-Rock Interactions.

Vincendon, M., Pilorget, C., Carter, J., & Stcherbinine, A. (2018). Observational evidence for a dry dust-wind origin of Mars seasonal dark flows. https://arxiv.org/abs/1808.09699v1

Viviano-Beck, C. E., et al. (2015). MRO CRISM type spectra library. Retrieved from http://crismtypespectra.rsl.wustl.edu

Wiseman, S., Arvidson, R., Wolff, M., Smith, M., Seelos, F., Morgan, F., Murchie, S. L., et al. (2016). Characterization of artifacts introduced by the empirical volcano-scan atmospheric correction commonly applied to CRISM and OMEGA near-infrared spectra. *Icarus*, *269*, 111–121. https://doi.org/10.1016/j.icarus.2014.10.012

Wray, J., Murchie, S., Ehlmann, B., Milliken, R., Seelos, K., Noe Dobrea, E., et al. (2011). Evidence for regional deeply buried carbonate-bearing rocks on Mars. Paper Presented at the Lunar and Planetary Science Conference.

Yerebakan, H. Z., Rajwa, B., & Dundar, M. (2014). The infinite mixture of infinite Gaussian mixtures. Paper presented at the Advances in neural information processing systems.